biomechanics

MDPI

Article

Impact of Contralateral Hemiplegia on Lower Limb Joint Kinematics and Dynamics: A Musculoskeletal Modeling Approach

Sadia Younis [1], Alka Bishnoi [2], Jyotindra Narayan [3,4,5,*] and Renato Mio [6]

[1] Department of Biomedical Engineering, Government College of Engineering and Technology Safapora, Ganderbal 193504, Kashmir, India; sadiyabhatt010@gmail.com
[2] Department of Physical Therapy, College of Health Professions and Human Services, Kean University, Union, NJ 07083, USA; abishnoi@kean.edu
[3] Department of Mechanical Engineering, Thapar Institute of Engineering and Technology, Patiala 147004, Punjab, India
[4] Department of Computing, Imperial College London, London SW7 2RH, UK
[5] Department of Mechanical Engineering, Indian Institute of Technology Guwahati, Guwahati 781039, Assam, India
[6] Digital Health, Universität Bayreuth, 95326 Kulmbach, Germany; renato.mio-zaldivar@uni-bayreuth.de
* Correspondence: n.jyotindra@gmail.com or jnarayan@ic.ac.uk

Abstract: This study investigates the biomechanical differences between typically developed (TD) individuals and those with contralateral hemiplegia (CH) using musculoskeletal modeling in OpenSim. Ten TD participants and ten CH patients were analyzed for joint angles and external joint moments around the three anatomical axes: frontal, sagittal, and transverse. The analysis focused on hip, pelvis, lumbar, knee, ankle, and subtalar joint movements, leveraging MRI-derived bone length data and gait analysis. Significant differences ($p < 0.05$) were observed in hip flexion, pelvis tilt, lumbar extension, and ankle joint angles, highlighting the impact of hemiplegia on these specific joints. However, parameters like hip adduction and rotation, knee moment, and subtalar joint dynamics did not show significant differences, with $p > 0.05$. The comparison of joint angle and joint moment correlations between TD and CH participants highlights diverse coordination patterns in CH. Joint angles show significant shifts, such as HF and LR (-0.35 to -0.97) and PR and LR (0.22 to -0.78), reflecting disrupted interactions, while others like HR and LR (0.42 to 0.75) exhibit stronger coupling in CH individuals. Joint moments remain mostly stable, with HF and HA (0.54 to 0.53) and PR and LR (-0.51 to -0.50) showing negligible changes. However, some moments, like KA and HF (0.11 to -0.13) and PT and KA (0.75 to 0.67), reveal weakened or altered relationships. These findings underscore biomechanical adaptations and compensatory strategies in CH patients, affecting joint coordination. Overall, CH individuals exhibit stronger negative correlations, reflecting impaired coordination. These findings provide insight into the musculoskeletal alterations in hemiplegic patients, potentially guiding the development of targeted rehabilitation strategies.

Keywords: biomechanical differences; contralateral hemiplegia; musculoskeletal modeling; OpenSim; gait analysis; significant differences; joint kinematics; joint moments; rehabilitation strategies

Citation: Younis, S.; Bishnoi, A.; Narayan, J.; Mio, R. Impact of Contralateral Hemiplegia on Lower Limb Joint Kinematics and Dynamics: A Musculoskeletal Modeling Approach. *Biomechanics* **2024**, *4*, 784–804. https://doi.org/10.3390/biomechanics4040058

Academic Editors: Gabriëlle Tuijthof and Malte Asseln

Received: 13 October 2024
Revised: 7 December 2024
Accepted: 12 December 2024
Published: 18 December 2024

1. Introduction

Musculoskeletal models are computational representations of the human musculoskeletal system designed to simulate the biomechanics of muscles, bones, and joints [1]. These models serve as critical tools in understanding human movement and diagnosing, treating, and preventing various disorders [2,3]. They incorporate anatomical data and dynamic principles to replicate the physical and physiological characteristics of the body, providing insights into how different muscles and joints contribute to movement and stability. Researchers and clinicians utilize these models to analyze complex movements, assess musculoskeletal health, and develop rehabilitation strategies [4]. Musculoskeletal

analysis shows promise as a valuable tool for forecasting outcomes in orthopedic surgeries and fine-tuning assistive devices [5].

Changes in any aspect of natural brain activity can contribute to neurological conditions such as cerebral palsy (CP) and stroke [6]. These conditions can impact the human skeletal system both directly and indirectly, leading to various abnormalities. Cerebral palsy manifests as a diverse clinical syndrome caused by brain injuries during prenatal or neonatal periods, affecting muscle tone, movement, and motor abilities. Conversely, stroke occurs when there is a sudden interruption or decrease in blood flow to the brain. After a stroke, individuals may experience paralysis in different parts of the body, which may lead to hemiplegia, paraplegia, or quadriplegia, depending on the affected limb. Contralateral hemiplegia (CH) is a form of hemiplegia that affects one side of the body opposite to the side of the brain or spinal cord injury that causes paralysis [7,8]. The severity of contralateral hemiplegia can vary, and it significantly influences skeletal dimensions in older adults [8,9], leading to leg length discrepancy (LLD). In several patient groups, LLD has been linked to compensatory gait abnormalities and can lead to degenerative arthritis in the lower extremities and spine [10,11]. The cause of LLD in CH is unclear, but it may result from a brain injury affecting growth on the hemiplegic side or disuse of the limb. Gait analysis shows that the hemiplegic foot bears less weight and generates less muscle work than the unaffected side, reducing the load on the growth plates and impacting limb development [11].

OpenSim, developed by Stanford University, is a widely used open-source software that allows researchers to build, analyze, and visualize musculoskeletal models [12,13]. This tool was selected for the present study due to its extensive documentation, active user community, and robust capabilities for simulating and analyzing musculoskeletal dynamics, which align with the objectives of this research. Customizing the selection of software according to specific study or application needs is crucial. The potential impact of musculoskeletal modeling and simulation on patient care and reducing treatment costs is substantial, examining causal connections in individuals with neurological and musculoskeletal impairments and forecasting successful rehabilitation results. This enables researchers to perform detailed biomechanical analyses and simulate the impact of different interventions, facilitating the development of personalized treatment plans and improving patient outcomes. OpenSim has been extensively applied in modeling lower-limb biomechanics, analyzing joint kinematics, and exploring the effects of various conditions on human movement [14–17].

This study is rooted in the premise that contralateral hemiplegia (CH) introduces significant biomechanical alterations in lower-limb joint kinematics and dynamics, which can impact mobility and quality of life. While musculoskeletal modeling using OpenSim provides a robust framework for analyzing these effects, previous research has not adequately explored how CH affects joint coordination and its biomechanical implications compared to typically developed (TD) individuals. This gap motivates our hypothesis that CH disrupts joint angles and external moments in distinct patterns, warranting a systematic investigation. By leveraging OpenSim's advanced simulation tools, this research aims to elucidate these biomechanical differences, establish statistical correlations, and propose evidence-based rehabilitation strategies, thereby bridging the current knowledge gap in post-hemiplegic musculoskeletal analysis. This study, specifically, delved into the impact of CH on joint angles and moments in sagittal, frontal, and transverse planes, comparing the findings to those of TD individuals. Ten patients diagnosed with CH, with a median age of 46 years (ranging from 39 to 52 years), were included in this study. Additionally, ten TD individuals with similar body characteristics were recruited as controls. The main contributions of the work are as follows:

(i) To investigate biomechanical differences in joint angles and moments between contralateral hemiplegia (CH) patients and typically developed (TD) individuals using OpenSim tools.

(ii) To analyze these differences statistically using mean absolute deviation, box plots, *t*-tests, and correlation analysis and provide insights into joint coordination to guide rehabilitation strategies.

2. Materials and Methods

2.1. Data Collection

This study involved 10 individuals diagnosed with contralateral hemiplegia, with a median age of 46 years (range: 39 to 52 years), a weight of 72.5 ± 5.5 kg, and a height of 1.75 ± 0.6 m. Among these participants, 7 were male and 3 were female. All were classified as gross motor function classification scale (GMFCS) 2 and as type 1 or 2 in the Winters classification based on sagittal plane kinematics from gait analysis [18]. Each individual had a Wisconsin gait scale (WGS) [19] score greater than 28, as determined by a comprehensive gait analysis that included 14 measurements conducted by the University of Wisconsin. In addition, this study included 10 age-matched TD controls. Exclusion criteria for the control group included a history of lower-extremity bone surgery or fractures and the presence of metal implants that would contraindicate MRI examinations. Participants with intellectual disability were also excluded. The measurements of pelvic, femur, tibia, talus, and calcaneus lengths for all participants, as detailed in Table 1, were derived from existing high-resolution MRI reports. These MRI records were sourced from medical imaging databases and neuromuscular clinics of Sheosagar Paralysis and Polio Hospital in Bihar, India, ensuring precision and consistency across all subjects. The data were critical for calculating the relative differences in bone lengths between contralateral hemiplegia (CH) patients and typically developed (TD) individuals. These relative differences were then used to refine and adjust the scale factors in the OpenSim Gait2392 model, ensuring the models accurately reflected the biomechanical characteristics of both groups. Ethical approval was obtained for the use of these existing MRI reports, and informed consent was secured from the respective participants, adhering to all relevant ethical guidelines for data usage. Institutional review board approval was obtained from Indian Institute of Technology Guwahati ethics committee for research involving both TD and affected individuals.

Table 1. Mean ± SD length of calcaneus, talus, tibia, femur, and pelvis for CH patients and TD controls.

Bone	Length CH Affected (mm)	Length TD (mm)	Relative Difference for Mean Length (%)
Calcaneous	42.3 ± 0.8	43.1 ± 0.9	98.1
Talus	32.1 ± 0.6	32.8 ± 0.8	97.8
Tibia	349.0 ± 3.6	377.12 ± 4.1	92.38
Femur	437.8 ± 5.8	455.7 ± 6.1	96.1
Pelvis	116.1 ± 1.3	115.6 ± 1.1	100.5

2.2. Adopted Methodolgy

The utilization of the Gait2392 model within OpenSim proved crucial for this research study. This model includes lower-limb structures, as well as the head and torso, constituting 12 segments, 11 joints, and 92 muscle–tendon actuators. Specifically, it comprises 72 muscles from the lower extremities and torso, facilitating a total of 23 degrees -of-freedom (DOF). Subject-specific characteristics, such as a mass of 75.16 kg and a height of 1.8 m, were specified [10]. Upon loading the scale file, OpenSim automatically generated scale factors for various body parts based on a TD subject, aligning with the mean bone length values of controls in the study. Since the standard deviations of bone lengths were minimal, indicating limited variability within each group, the mean bone lengths of all subjects (TD and CH) were used to alter the scale factors in OpenSim. This approach, while computationally efficient, is also aligned with modeling practices for group-level analyses where participant differences are small. Gait analysis was conducted through inverse kinematics and inverse

dynamics, allowing for a thorough comparison of gait parameters between TD and CH conditions. The detailed process for gait analysis in OpenSim, encompassing both TD and CH conditions, is described below.

2.2.1. Model for TD Subjects

To start, the Gait2392 model was opened in OpenSim, where the scale tool was used to import the *Subject01-Setup-Scale.xml* file—an accessible setup file offering insights into the gait cycle of a typical TD model with details of virtual marker set and a tag to experimental marker set in static pose. *Subject01-Static.trc*, having details of experimental markers trajectories, was used to include the full marker set in static pose. The experimental marker data were recorded by John et al. [20] using a six-camera motion capture system every 1/60 s intervals. Upon loading the files, a revised model *Subject01-Simbody.osim* appeared, weighing 72.6 kg and featuring a total of 39 markers. Table 2 displays the scale factors for different body segments on the right side, reflecting comparable measurements for the left side under TD conditions. The manual scales provided insights into the scale adjustments for the new model in comparison to the standard Gait2392 model.

Table 2. Scale Factor for TD model using OpenSim.

Bone	Measurement Used	Scale Factor
Calcaneus (R)	Foot	1.027085
Talus (R)	Shank	1.113978
Tibia (R)	*Manual scales* *	0.988523
Femur (R)	*Manual scales*	1.147240
Toes (R)	Foot	1.027085
Pelvis	Pelvis	1.024577

* Manual scales in italics represent the manual adjustments of scale factors over the Gait2392 model.

Following this, inverse kinematics were calculated using the scaled model via the corresponding tool, as illustrated in Figure 1a. The *Subject01-Setup-IK.xml file* was loaded with a tag to the experimental marker set as *Subject01-Walk1.trc*, and the program was run within a defined time span of 0 to 2.5 s. *Subject01-Walk1.trc* was used to include experimental marker data for a trial obtained from the motion capture system, along with the time range of interest, as per the study by John et al. [20]. This generates a motion file, *Subject01-Walk1-IK.mot*, having the time histories of generalized coordinates that describe the movement of the TD model. The objective of the analysis was to assess the variation in angles (including hip flexion, adduction, rotation, lumbar bending, extension, rotation, knee angle, ankle angle, and subtalar joint angles) over the specified timeframe. After that, inverse dynamics were calculated using the scaled model via the corresponding tool, as illustrated in Figure 1b. *Subject01-Setup-ID.xml*, with a tag to inverse kinematics-based motion file, was loaded. Moreover, an external loads setup file, *Subject01-Walk1-GRF.xml*, was uploaded to measure and apply or model all external forces acting on a subject during the motion to calculate accurate joint torques and forces [20,21]. This file includes the name of the ground reaction force data file (*Subject01-GRF.mot*) as well as the names of the bodies to which they are applied. Finally, the program was run within a predefined time span of 0 to 2.5 s, and *InverseDynamics-TD.sto* file was saved to obtain the relevant plots The objective of the analysis was to assess the changes in joint moments over the specified timeframe.

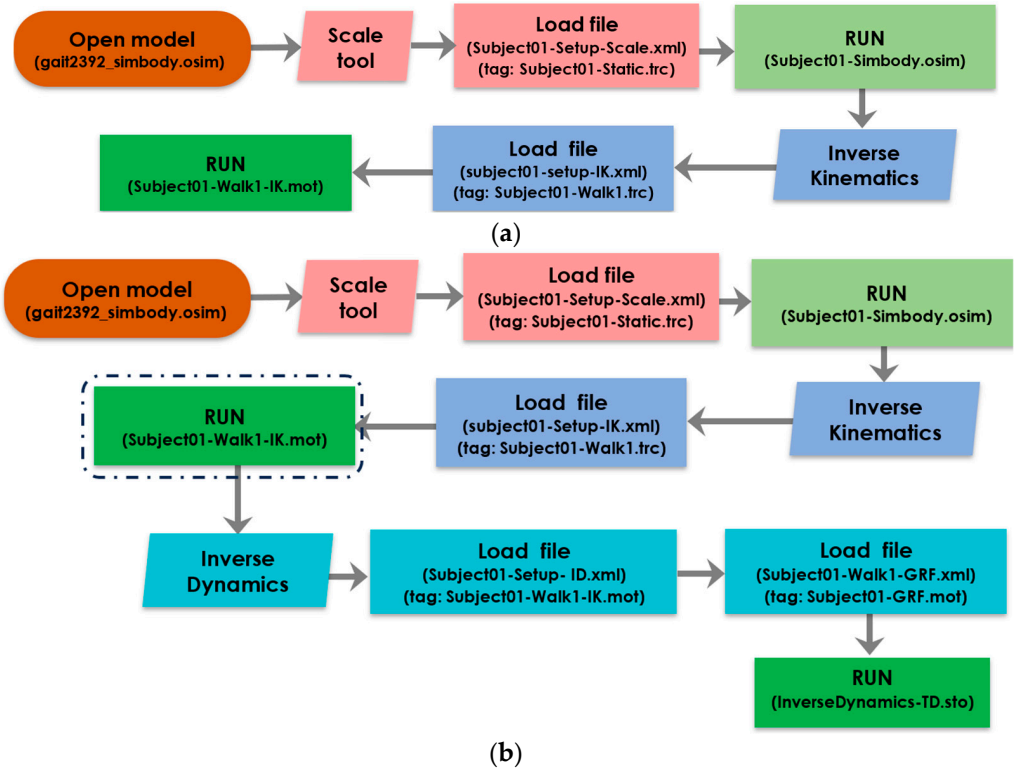

Figure 1. Process flow to run (**a**) IK for scaled TD model in OpenSim and (**b**) ID for scaled TD model in OpenSim (dotted run block represents the significance of IK compilation before initiating the process of ID).

2.2.2. Model for CH-Affected Subjects

In the initial step of this study, the Gait2392 model was utilized within the OpenSim platform. Similar to the approach for the TD model, the scale tool was used to load the *Subject01-Setup-Scale.xml* file having a tag to experimental marker set (*Subject01-Static.trc*) in static pose, resulting in the generation of the model with a mass of 72.6 kg and a total of 39 markers. Afterward, the relative differences from Table 1 were divided by 100, and the resultant values were then multiplied by the respective scale factors listed in Table 2. This procedure resulted in the development of an altered model depicting a CH state, *Subject01-Simbody-CH.osim*, specifically designed to represent the CH condition. The modified scale factors for the right side (R) were detailed in Table 3, while the scale factors for the left side remained the same as those for the scaled TD model. Notably, from Table 3, it is evident that all measurements, except those for the toes, were manually adjusted. The revised scale file was stored and loaded under the name *Subject01-setup-scale-CH.xml* for future reference, as illustrated in Figure 2a. Subsequently, the inverse kinematics tool was utilized on the scaled model by loading the *Subject01-Setup-IK.xml* file with a tag to with a tag to the experimental marker set as *Subject01-Walk1.trc* and running the program within the designated time frame of 0 to 2.5 s. It is pertinent to mention that the experiment marker set, *Subject01-Walk1.trc*, used here is the same as mentioned in Section 2.2.1. However, due to the positional differences between CH's virtual marker set and TD's experimental marker set, the program generates a new motion file, *Subject01-Walk1-IK-CH.mot*, having the time histories of generalized coordinates that describe the movement of the CH model.

Following that, the gait kinematics of various body joints, such as hip flexion, hip adduction, hip rotation, lumbar bending, lumbar extension, lumbar rotation, knee angle, ankle angle, and subtalar angle joints, were examined using inverse kinematics for the CH model. Inverse dynamics were calculated using the scaled model via the inverse dynamics tool as shown in Figure 2b. *Subject01-Setup-ID.xml*, with a tag to inverse kinematics-based motion file, was loaded. Moreover, similar to Section 2.2.1, external loads setup file,

Subject01-Walk1-GRF.xml with a tag to *Subject01-GRF.mot*, was uploaded to measure and apply or model all external forces acting on a subject during the motion to calculate accurate joint torques and forces [20,21]. Finally, the program was run within a predefined time span of 0 to 2.5 s, and the *InverseDynamics-CH.sto* file was saved to show the relevant plots. The respective lower limb joint moments were obtained over the specified timeframe.

Table 3. Scale factor for CH model using OpenSim.

Bone	Measurement Used	Scale Factor
Calcaneus (R)	*Manual scales* *	1.00757
Talus (R)	*Manual scales*	1.08947
Tibia (R)	*Manual scales*	0.913197
Femur (R)	*Manual scales*	1.102497
Toes (R)	Foot	1.027085
Pelvis	*Manual scales*	1.029699

* Manual scales in italics represent the manual adjustments of scale factors over the Gait2392 modelmodel.

Figure 2. Process flow to run (**a**) IK for CH model in OpenSim and (**b**) run ID for CH (CH) model in OpenSim (dotted run block represents the significance of IK compilation before initiating the process of ID).

Figure 3 elucidates the experimental markers (orange, light colored) for the mean TD participant and the virtual markers (black, dark colored) for the mean CH patient after scaling, representing key anatomical landmarks. The utility of these marker sets

lies in their critical role in evaluating joint kinematics and dynamics using OpenSim, derived from the relative differences between the marker sets. These relative differences in marker positions were used to adjust the scale factors in the OpenSim Gait2392 model, as shown in Tables 2 and 3, ensuring that the musculoskeletal models accurately reflected the biomechanical characteristics of each group. The inverse kinematics (IK) and inverse dynamics (ID) computations were then performed using these scaled models to analyze and compare joint movements and forces between the TD and CH groups.

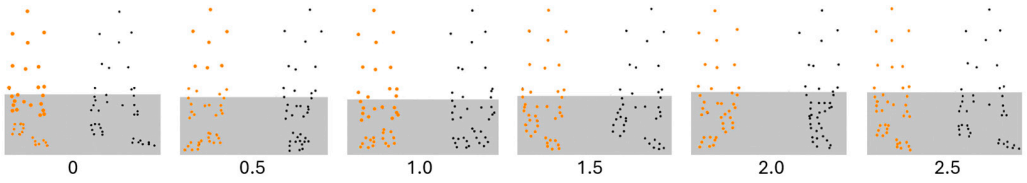

Figure 3. Experimental (orange, light colored, left side) marker sets for the mean TD participant and virtual (black, dark colored, right side) marker sets for the mean CH patient for 0–2.5 s.

3. Results and Discussions

This Section presents comprehensive results on the effect of altered leg length for joint kinematics and dynamics post CH and compares with the kinematics and dynamics of TD subjects. Moreover, it also discusses correlation analysis for joint angles and moments with TD participants and CH-affected subjects.

3.1. Kinematics

3.1.1. Hip Joint

Hip flexion, as depicted in Figure 4a, showcases the absolute deviation between hip joint angles of TD and CH (CH) conditions, with an absolute mean deviation of 8.04°, indicating notable differences in distribution. In the TD dataset, the median angle is 6.77° with an IQR from −11.59 to 19.08°, while the CH dataset shows a higher median of 13.71° and an IQR from −2.39 to 26.76°, suggesting increased variability and higher angles in CH condition. Similarly, in hip adduction (Figure 4b), the absolute mean deviation is 0.48°, indicating relatively little difference between TD and CH conditions. The TD dataset shows a median of −0.94° with an IQR from −4.11 to 3.58°, while the CH dataset displays a median of −1.41° with an IQR from −4.85 to 2.92°. Furthermore, in hip rotation (Figure 4c), the absolute mean deviation is 0.45°, indicating a moderate difference between TD and CH datasets. The TD dataset's median angle is −4.35° with an IQR from −6.71 to 0.39°, whereas the CH dataset's median is −3.69° with an IQR from −6.20 to 0.55°.

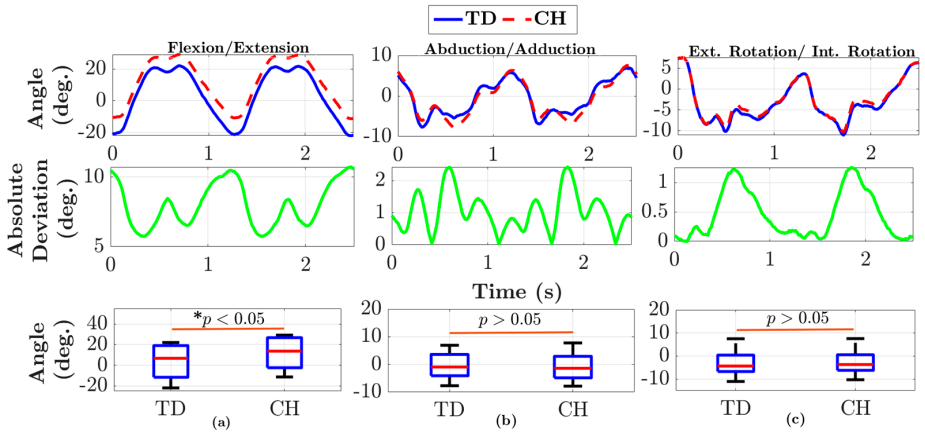

Figure 4. Comparison between TD and CH hip (**a**) flexion angle, absolute deviation and box-plot; (**b**) adduction angle, absolute deviation and box-plot; and (**c**) rotation angle, absolute deviation and box-plot (* represents statistically significant differences).

3.1.2. Pelvis Bone

In pelvis tilt, as illustrated in Figure 5a, the absolute mean deviation of 8.0193° underscores significant variability between TD and CH conditions, supported by pronounced distribution disparities evident in box plot analysis. TD pelvis tilt data exhibit a median of −4.89° with an interquartile range (IQR) from 4.54° to 5.35°, implying a tighter spread, whereas the CH dataset displays a median of −3.18° with an IQR from −3.51° to −2.62°, indicating a comparably narrow distribution. In pelvis rotation, depicted in Figure 5b, the absolute mean deviation of 0.25° suggests minimal variation between TD and CH (CH) individuals, corroborated by the analogous patterns observed in box plot analysis. TD pelvis rotation data portray a median of −0.64° with an IQR from −3.55° to 1.43°, indicating moderate dispersion, while the CH dataset showcases a median of −0.55° with an IQR from −3.69° to 1.97°, suggesting moderate to substantial dispersion.

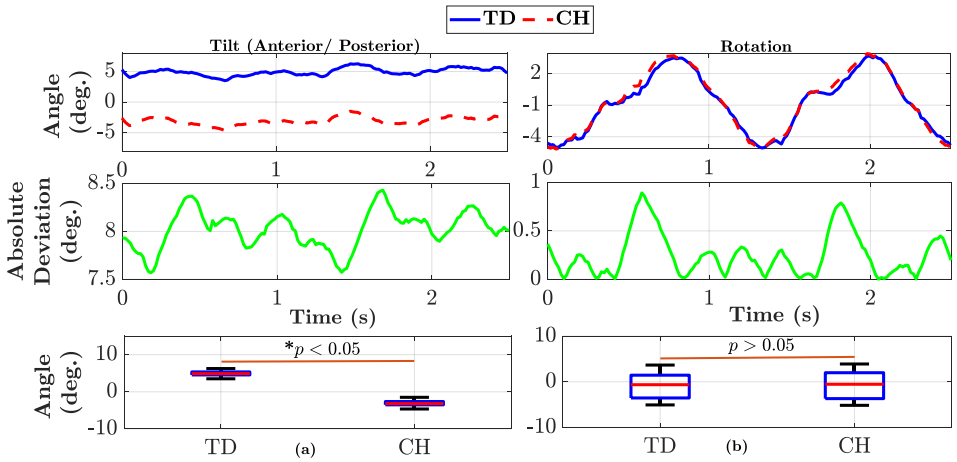

Figure 5. Comparison between TD and CH pelvis (**a**) tilt angle, absolute deviation and box-plot and (**b**) rotation angle, absolute deviation and box-plot (* represents the differences are statistically significant).

3.1.3. Lumbar Joint

Lumbar extension (Figure 6a) shows a larger absolute mean deviation of 1.4161°, indicating substantial differences in distribution between TD and CH angles. For TD lumbar extension, the median is −15.88°, with an IQR from −15.19° to −16.58°, indicating moderate spread, while the CH dataset exhibits a median of 17.52° with an IQR from −16.65° to −17.95°, representing a narrower spread. In lumbar rotation (Figure 6b), the absolute mean deviation of 0.39° suggests relatively little difference between TD and CH individuals, with TD lumbar rotation data showing a median of −2.07° and an IQR from −6.01° to 2.59°, indicating wider spread, while the CH dataset displays a median of −2.22° and an IQR from −6.32° to 2.55°, suggesting a moderate to substantial dispersion. In lumbar bending, as depicted in Figure 6c, the absolute mean deviation of 0.7844° underscores significant differences between TD and CH conditions, with notable distribution variations observed in box plot analysis. For TD lumbar bending, the median angle is −0.12° with an interquartile range (IQR) from −2.75° to 2.32°, while the CH dataset shows a median of 0.09° with an IQR from −2.35° to 2.45°, suggesting relatively narrow spread. These results underscore the complex biomechanical differences between TD and CH states in lumbar bending, extension, and rotation, emphasizing the importance of statistical analyses in clarifying these subtleties.

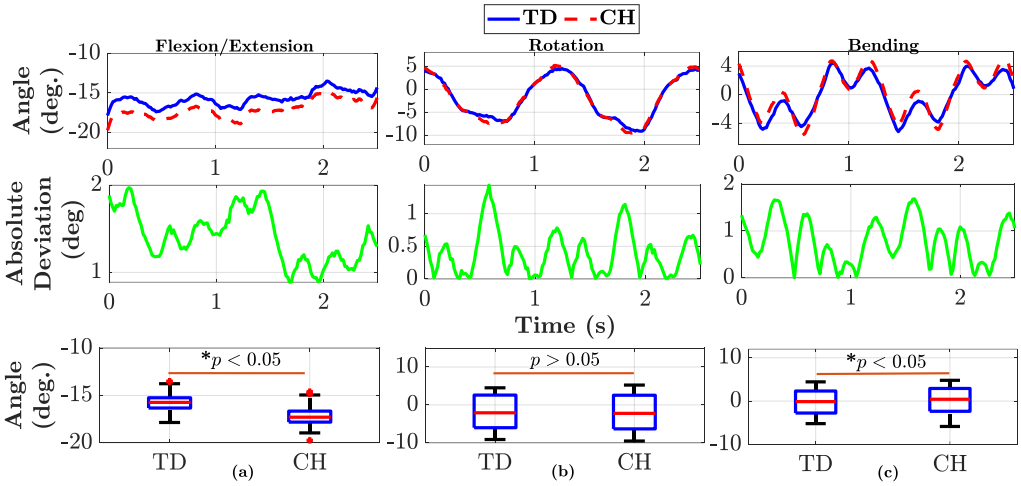

Figure 6. Comparison between TD and CH lumbar: (**a**) flexion angle, absolute deviation and box-plot; (**b**) adduction angle, absolute deviation and box-plot; and (**c**) rotation angle, absolute deviation and box-plot (* represents the differences are statistically significant).

3.1.4. Knee Joint Angle

The knee joint angle in the sagittal plane for both TD and CH (CH) conditions is depicted in Figure 7. Moreover, it illustrates the absolute deviation between the knee joint angles of TD and CH (CH) conditions. The absolute mean deviation between TD and CH knee joint angles is computed to be 1.378°. The relatively small absolute mean deviation suggests that, on average, the disparities in knee joint angles between TD and CH conditions are minimal. Box plot analysis comparing TD and CH knee joint angles reveals distinct distribution patterns. For TD knee joint angles, the median is −18.84°, indicating the central tendency of the data. The interquartile range (IQR) spans from the lower quartile of −38.71° to the upper quartile of −8.51°, indicating a concentrated distribution of values. The upper whisker reaches 0.97°, while the lower whisker extends to −69.76°, suggesting a relatively symmetrical distribution with a moderate spread of data. In contrast, CH knee joint angles exhibit a median of −18.91°, indicating a similar central tendency to the TD group. The IQR extends from the lower quartile of −37.95° to the upper quartile of −9.53°, showcasing a comparable concentrated distribution. The upper whisker reaches 1.35°, and the lower whisker extends to −70.46°, reflecting a symmetrical distribution with a slightly wider spread compared to the TD condition. Overall, the box plots visually illustrate similarities in central tendencies and distributions between TD and CH knee joint angles.

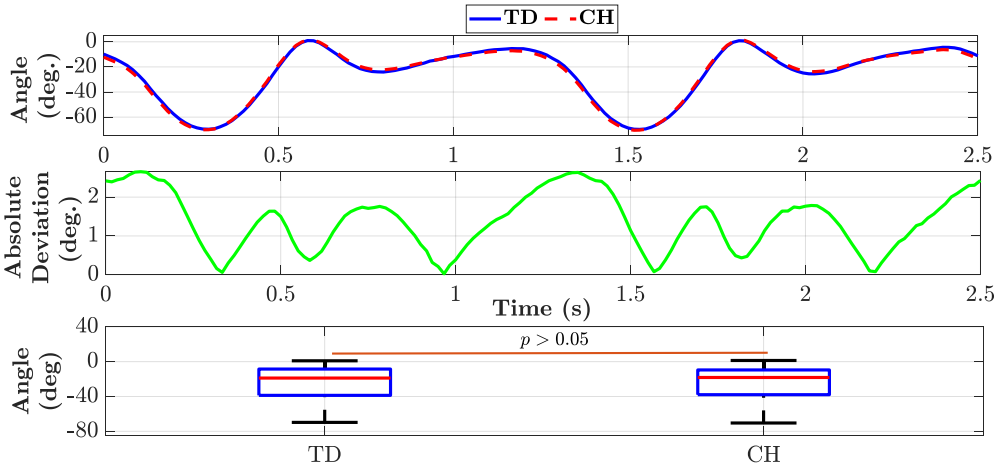

Figure 7. Comparison between TD and CH knee angle, absolute deviation, and box-plot analysis.

3.1.5. Ankle Joint Angle

Figure 8 displays the ankle joint angles for both TD and CH (CH) conditions in the sagittal plane. Moreover, the disparity in ankle joint angles is depicted in Figure 8, demonstrating the absolute deviation between the TD and CH (CH) ankle joint angles. The absolute mean deviation, measuring the average absolute difference in ankle joint angles between TD and CH conditions, is calculated to be 4.51°. The relatively large absolute mean deviation suggests that, on average, substantial differences exist in ankle joint angles between TD and CH conditions. Box plot analysis comparing TD and CH ankle joint angles reveals significant distribution differences, as demonstrated in Figure 8. In the TD ankle joint angle dataset, the median is 2.68°, with an interquartile range (IQR) from 0.94° to 9.4°, indicating a concentrated distribution. The upper whisker extends to 16.02°, while the lower whisker reaches −8.84°, reflecting moderate variability. This suggests a relatively symmetrical distribution with a noticeable spread of data. Conversely, the CH ankle joint angles display a distinct distribution, with a median of 8.23° and an IQR from 4.60° to 13.3°. The upper whisker reaches 20.62°, and the lower whisker extends to −1.4°, indicating a broader spread and a potential skewness towards higher angles (less ankle plantarflexion). In summary, the box plots visually depict considerable discrepancies in ankle joint angles between TD and CH conditions, with the statistical analysis bolstering the conclusion of a substantial dissimilarity. These findings emphasize the significance of incorporating both visual representation and statistical testing to comprehensively comprehend the variations in ankle joint angles between the two groups.

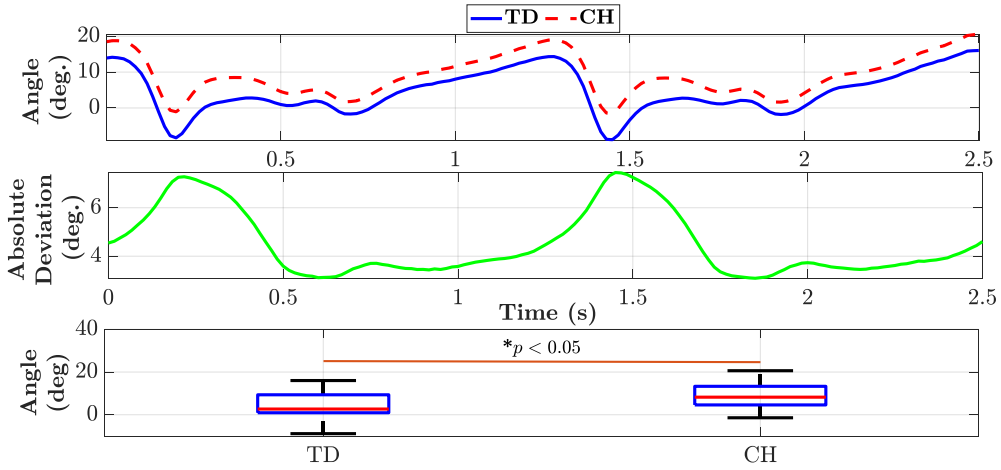

Figure 8. Comparison between TD and CH ankle angle, absolute deviation, and box-plot (* represents the differences are statistically significant).

3.1.6. Subtalar Joint Angle

Figure 9 depicts the subtalar joint for both TD and CH conditions in the sagittal plane. The disparity in subtalar joint is illustrated in Figure 9, showcasing the absolute deviation between the TD and CH subtalar joint. The absolute mean deviation, quantifying the average absolute difference in subtalar joint between TD and CH conditions, is determined to be $3.98 \times 10^{-7\circ}$. This significantly small absolute mean deviation implies much less variability in the subtalar joint measurements between TD and CH individuals. The box plot analysis comparing TD and CH subtalar joints reveals significant distribution differences, as illustrated in Figure 9. In the TD subtalar joint data, the median is $-1.52 \times 10^{-6\circ}$, with an IQR from $-3.38 \times 10^{-6\circ}$ to $-7.25 \times 10^{-7\circ}$, which implies a more compact distribution (narrow spread), indicating that the data points are closely grouped together. The upper whisker extends to $3.25 \times 10^{-6\circ}$, and the lower whisker reaches $-7.36 \times 10^{-6\circ}$. Most of the data are probably tightly clustered within a narrow range, implying minimal variability. However, the existence of outliers or extreme values beyond the whiskers may hint at some degree of variability in the dataset. Conversely, the CH subtalar joint angles exhibit a

different distribution, with a median of $-1.27 \times 10^{-6\circ}$ and an IQR from $-3.10 \times 10^{-6\circ}$ to $-4.22 \times 10^{-6\circ}$, which suggests that the data are spread across relatively narrow range. The upper whisker reaches $-3.60 \times 10^{-6\circ}$, and the lower whisker extends to $-7.12 \times 10^{-6\circ}$, showing limited variability.

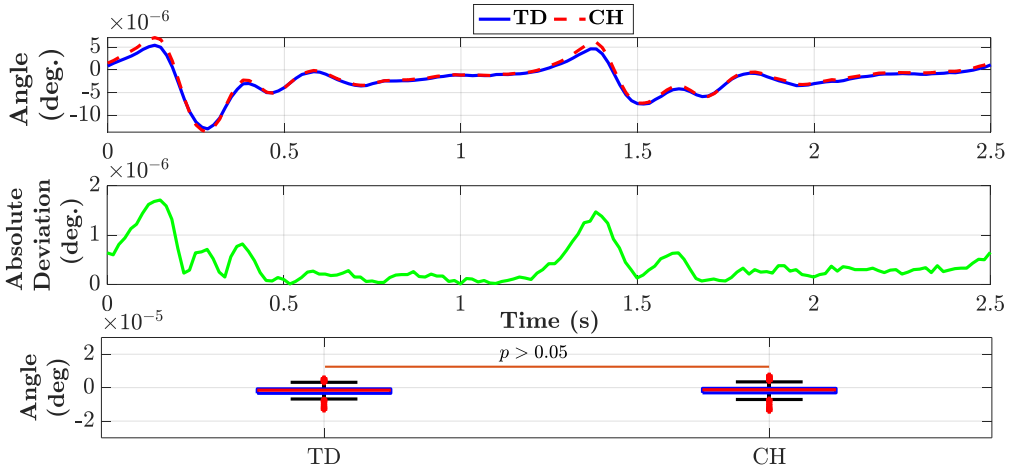

Figure 9. Comparison between TD and CH subtalar angle, absolute deviation, and box-plot.

Consolidating all the above outcomes in Table 4 and performing *t*-test, the *p*-values highlight significant and non-significant biomechanical differences in joint movements between typically developed (TD) and contralateral hemiplegia (CH) participants. Statistically significant differences ($p < 0.05$) were observed in hip flexion, pelvis tilt, lumbar extension, lumbar bending, and ankle flexion, indicating meaningful disparities in these motions between the two groups. These findings suggest altered kinematics in CH individuals, likely reflecting compensatory mechanisms or impaired coordination. On the other hand, motions such as hip adduction, hip rotation, pelvis rotation, lumbar rotation, knee flexion, and subtalar flexion exhibited $p > 0.05$, indicating no statistically significant differences between TD and CH groups for these parameters. These results provide insight into specific joints and motions where CH significantly impacts biomechanics, while others remain relatively unaffected, thus guiding targeted interventions and rehabilitation strategies.

Table 4. Statistical outcomes for TD and CH gait kinematics.

Joint and Motion	Median (TD)	IQR (TD)	Median (CH)	IQR (CH)	*p*-Value
Hip Joint					
Hip Flexion	6.77°	11.59–19.08°	13.71°	−2.39–26.76°	**<0.05 ***
Hip Adduction	−0.94°	−4.11–3.58°	−1.41°	−4.84–2.91°	>0.05
Hip Rotation	−4.34°	−6.71–0.39°	−3.69°	−6.20–0.56°	>0.05
Pelvis Bone					
Pelvis Rotation	−0.65°	−3.55–1.43°	−0.54°	−3.69–1.97°	>0.05
Pelvis Tilt	−4.89°	4.54–5.35°	−3.18°	−3.51–−2.62°	**<0.05**
Lumbar Joint					
Lumbar Extension	−15.88°	−15.19–−16.57°	−17.52°	−16.65–−17.95°	**<0.05**
Lumbar Rotation	−2.08°	−6.01–2.59°	−2.22°	−6.32–2.55°	>0.05
Lumbar Bending	−0.12°	−2.75–2.32°	0.09°	−2.35–2.45°	**<0.05**
Knee Joint					
Knee Flexion	−18.84°	−38.71–−8.51°	−18.91°	−37.95–−9.53°	>0.05

Table 4. *Cont.*

Joint and Motion	Median (TD)	IQR (TD)	Median (CH)	IQR (CH)	*p*-Value
Ankle Joint					
Ankle Flexion	2.68°	0.94–9.4°	8.23°	4.60–13.32°	**<0.05**
Subtalar Joint					
Subtalar Flexion	-1.52×10^{-6}°	-3.38×10^{-6}–-7.25×10^{-7}°	-1.27×10^{-6}°	-3.10×10^{-6}–-4.22×10^{-6}°	>0.05

* Bold numerals in the last column represent the statistical significant conditions with significance level of 0.05.

3.2. Correlation Analysis for Joint Kinematics

The heatmaps provided represent correlation matrices between various joint kinematic parameters for both TD and CH subjects. The joint parameters measured include hip flexion (HF), hip abduction (HA), hip rotation (HR), pelvis rotation (PR), pelvis tilt (PT), lumbar extension (LE), lumbar rotation (LR), lumbar bending (LB), knee angle (KA), ankle angle (AA), and subtalar angle (SA). The use of correlation matrices complements the boxplots and statistical analysis by offering a comprehensive view of kinematics interactions, which is crucial for understanding angular-position-related compensatory mechanisms in CH individuals.

The comparison of joint angle correlations between TD participants and CH patients, as shown in Figure 10, highlights significant differences, reflecting altered motor coordination and movement patterns in CH patients. For instance, the correlation between HF and LR changes from −0.35 in TD participants to −0.97 in CH patients, indicating a much stronger interdependence in CH. Similarly, the correlation between HR and LR increases from 0.42 in TD to 0.75 in CH, suggesting a closer relationship between these joint movements in CH patients. A striking shift is observed in the correlation between PR and LR, which changes from 0.22 in TD to −0.78 in CH, highlighting significant disruptions in their interaction. The negative sign represents that these movements occur in almost opposite phases in CH participants compared to TD. Other notable differences further emphasize altered biomechanics in CH patients. For example, the correlation between PT and LR increases from 0.01 in TD subjects to 0.31 in CH individuals. Additionally, the previously strong relationship between LR and LB, which is 1.00 in TD participants, weakens to 0.48 in CH patients.

In conclusion, the observed differences in joint angle correlations between TD participants and CH patients provide valuable insights into the altered motor coordination and biomechanical interactions in individuals with cerebral palsy. The significant shifts, such as the stronger coupling between certain joint pairs like HR and LR or the disrupted interactions between PR and LR, reflect compensatory mechanisms or neuromuscular impairments characteristic of CH patients. These findings underscore the complexity of motor control alterations in cerebral palsy and highlight the need for targeted rehabilitation strategies that address these specific joint dependencies.

3.3. Joint Dynamics

3.3.1. Hip Joint

Figure 11a shows hip flexion dynamics for TD and CH conditions in the sagittal plane, illustrating the absolute deviation between them. The box plot reveals the median TD hip flexion as −37.47 Nm, with an IQR from −44.81 Nm to 12.99 Nm. The upper and lower whiskers extend to 26.75 Nm and −83.87 Nm, respectively, indicating wide variability. For CH hip flexion, the median is −37.57 Nm, with an IQR from −45.82 Nm to 12.1 Nm, and whiskers extending to 31.81 Nm and −88.64 Nm, showing slightly greater variability. The *p*-value of 0.88 indicates no significant difference between TD and CH conditions. Figure 11b shows hip adduction dynamics for both conditions, also displaying the absolute deviation. The box plot reveals the median TD hip adduction as −9.22 Nm, with an IQR from −35.19 Nm to −0.48 Nm. The whiskers extend to 26.39 Nm and −52.12 Nm,

indicating wide variability. CH hip adduction has a median of −11.64 Nm, with an IQR from −36.46 Nm to 1.05 Nm, and whiskers extending to 24.88 Nm and −53.75 Nm, showing slightly greater variability. The *p*-value of 0.72 indicates no significant difference. Figure 11c shows hip rotation dynamics for both conditions, along with the illustration of the absolute deviation. The box plot reveals the median TD hip rotation as −0.99 Nm, with an IQR from −4.21 Nm to 1.55 Nm. The whiskers extend to 7.25 Nm and −12.84 Nm, indicating some variability. CH hip rotation has a median of −0.97 Nm, with an IQR from −4.05 Nm to 1.22 Nm, and whiskers extending to 7.70 Nm and −11.96 Nm, showing slightly less variability.

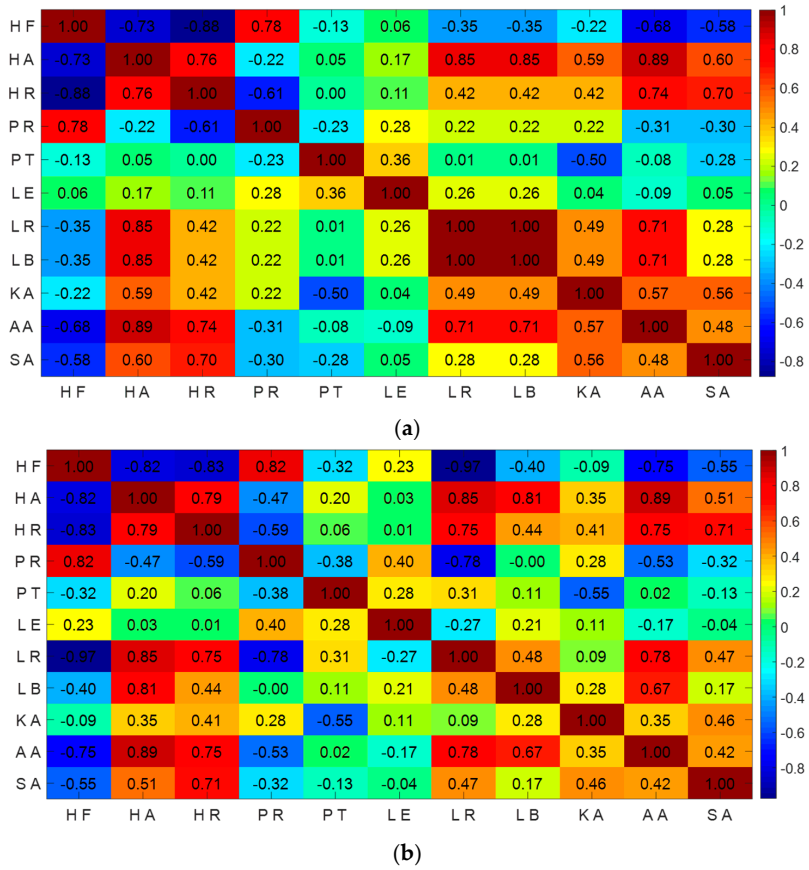

Figure 10. Correlation analysis for joint angles with (**a**) TD participants and (**b**) CH-affected subjects (− sign represents opposite phases between joints in the gait cycle).

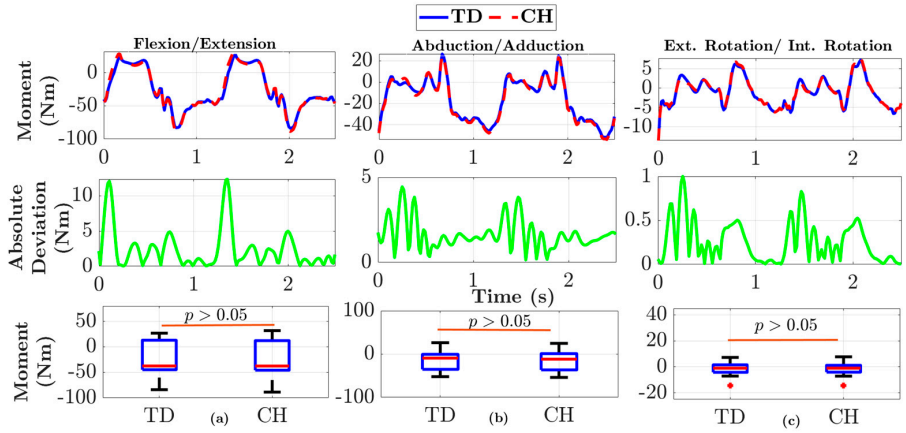

Figure 11. Comparison between TD and CH hip: (**a**) flexion moment, absolute deviation and box-plot; (**b**) adduction moment, absolute deviation and box-plot; and (**c**) rotation moment, absolute deviation and box-plot.

3.3.2. Pelvis Bone

Figure 12a depicts the pelvis rotation and tilt dynamics for both TD and CH conditions in the sagittal plane. The TD pelvis rotation, shown in Figure 12a, reveals a median of −0.35 Nm, with an IQR from −6.70 Nm to 5.81 Nm for TD pelvis rotation. The whiskers extend to 16.41 Nm and −16.85 Nm, indicating some variability within the dataset. Conversely, the CH pelvis rotation angles have a median of −0.83 Nm and an IQR from −7.48 Nm to 6.20 Nm. The whiskers extend to 17.31 Nm and −16.50 Nm, indicating slightly greater variability. The TD pelvis tilt, as shown in Figure 12b, presents a median of 38.71 Nm, with an IQR from 26.06 Nm to 47.12 Nm. The upper whisker extends to 57.59 Nm, and the lower whisker reaches −5.51 Nm, indicating considerable variability. The CH pelvis tilt angles exhibit a median of 43.62 Nm and an IQR from 31.71 Nm to 54.39 Nm. The upper whisker reaches 73.05 Nm, and the lower whisker extends to −1.66 Nm, indicating slightly greater variability in the CH dataset.

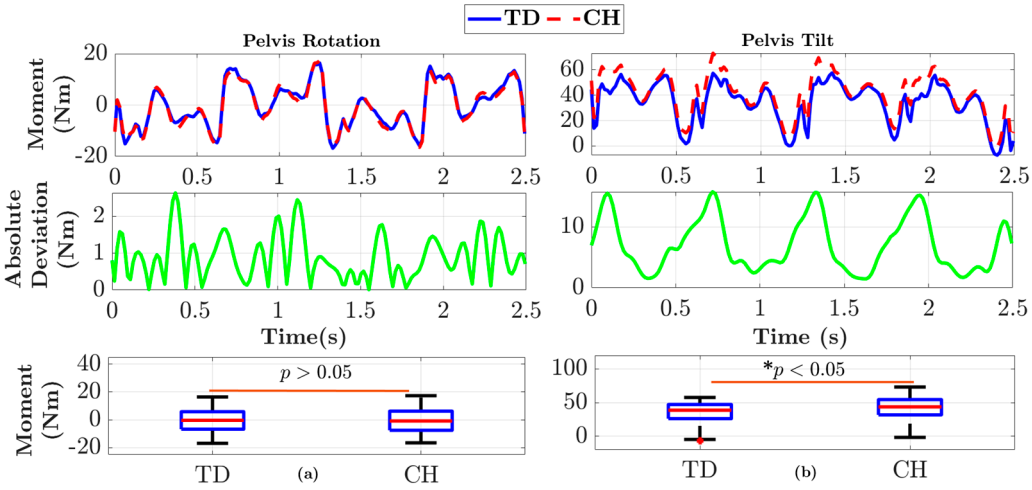

Figure 12. Comparison between TD and CH pelvis: (**a**) rotation moment, absolute deviation and box-plot; (**b**) tilt moment, absolute deviation and box-plot plot (* represents the differences are statistically significant).

3.3.3. Lumbar Joint

Figure 13a depicts lumbar extension dynamics. The box plot shows the median TD lumbar extension as 68.92 Nm, with an IQR from 58.54 Nm to 76.95 Nm, and whiskers extending to 85.90 Nm and 44.31 Nm. CH lumbar extension has a median of 74.38 Nm, an IQR from 62.89 Nm to 82.90 Nm, and whiskers extending to 93.98 Nm and 47.09 Nm, indicating significant differences. Similarly, Figure 13b illustrates lumbar rotation dynamics, showing the absolute deviation. The box plot reveals the median TD lumbar rotation as 0.88 Nm, with an IQR from −2.05 Nm to 2.72 Nm, and whiskers extending to 4.94 Nm and −3.54 Nm. CH lumbar rotation has a median of 0.87 Nm, an IQR from −2.29 Nm to 3.07 Nm, and whiskers extending to 5.64 Nm and −4.09 Nm. Figure 13c depicts the lumbar bending dynamics for both TD and CH conditions in the sagittal plane, showcasing the absolute deviation between them. The box plot analysis reveals the median TD lumbar bending as 5.22 Nm, with an IQR from −2.53 Nm to 15.26 Nm, and whiskers extending to 41.96 Nm and −29.23 Nm, indicating considerable variability. CH lumbar bending has a median of 5.99 Nm, an IQR from −3.30 Nm to 16.89 Nm, and whiskers extending to 47.19 Nm and −33.60 Nm, showing slightly greater variability.

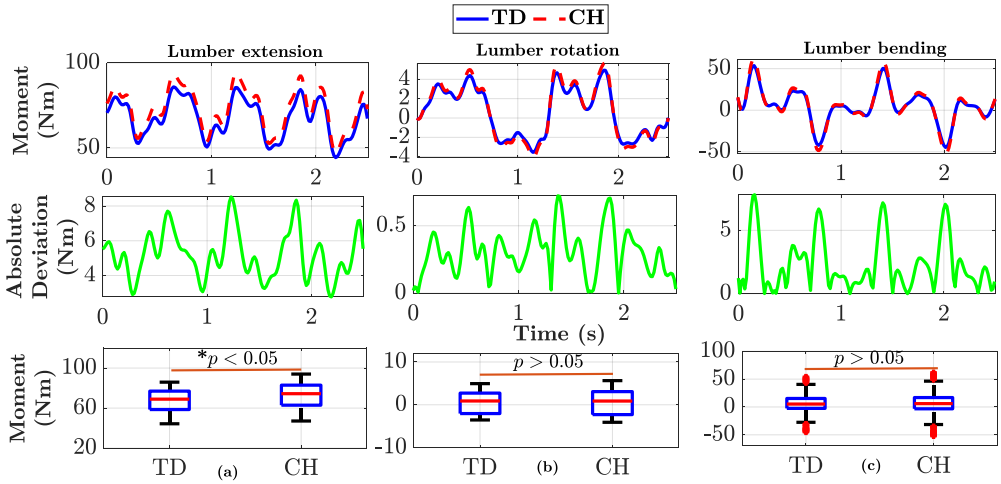

Figure 13. Comparison between TD and CH Lumbar: (**a**) extension moment, absolute deviation and box-plot; (**b**) rotation moment, absolute deviation and box-plot; and (**c**) bending moment, absolute deviation and box-plot (* represents the differences are statistically significant).

3.3.4. Knee Moment

Figure 14 illustrates the knee moment dynamics for both TD and CH conditions. The disparity in knee moment characteristics is depicted in Figure 14, showcasing the absolute deviation between the TD and CH knee moment values. The box plot analysis comparing TD and CH knee moments reveals distribution differences, as demonstrated in Figure 14. In the TD knee moment data, the median is −6.91 Nm, with an IQR from −21.53 Nm to 4.08 Nm, indicating a moderate distribution, suggesting that the data points are somewhat spread out. The upper whisker extends to 22.38 Nm, and the lower whisker reaches −34.71 Nm, indicating some variability within the dataset. Conversely, the CH knee moment values exhibit a similar distribution with a median of −4.07 Nm and an IQR from −19.44 Nm to 4.08 Nm, suggesting that the data are spread across a similar range. The upper whisker reaches 35.76 Nm, and the lower whisker extends to −33.17 Nm, indicating slightly greater variability in the CH dataset.

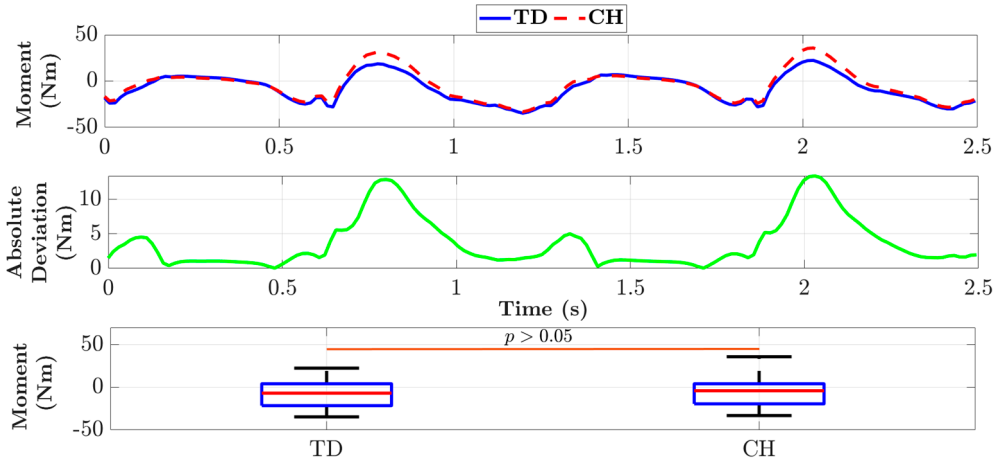

Figure 14. Comparison between TD and CH knee moment, absolute deviation, and box-plot.

3.3.5. Ankle Moment

Figure 15 illustrates the ankle moment dynamics for both TD and CH conditions. The disparity in ankle moment characteristics is depicted in Figure 15, showcasing the absolute deviation between the TD and CH ankle moment values. The box plot analysis comparing TD and CH ankle moments reveals distribution differences, as demonstrated in Figure 15. In the TD ankle moment data, the median is −39.14 Nm, with an interquartile range (IQR)

from −96.09 to 0.84 Nm, indicating a wide distribution and suggesting that the data points are spread out. The upper whisker extends to 2.41 Nm, and the lower whisker reaches −146.85 Nm, indicating considerable variability within the dataset. Conversely, the CH ankle moments exhibit a similar distribution with a median of −26.22 Nm and an IQR from −90.24 to 0.95 Nm, suggesting that the data are spread across a similar range. The upper whisker reaches 2.99 Nm, and the lower whisker extends to −140.68 Nm, indicating slightly greater variability in the CH dataset.

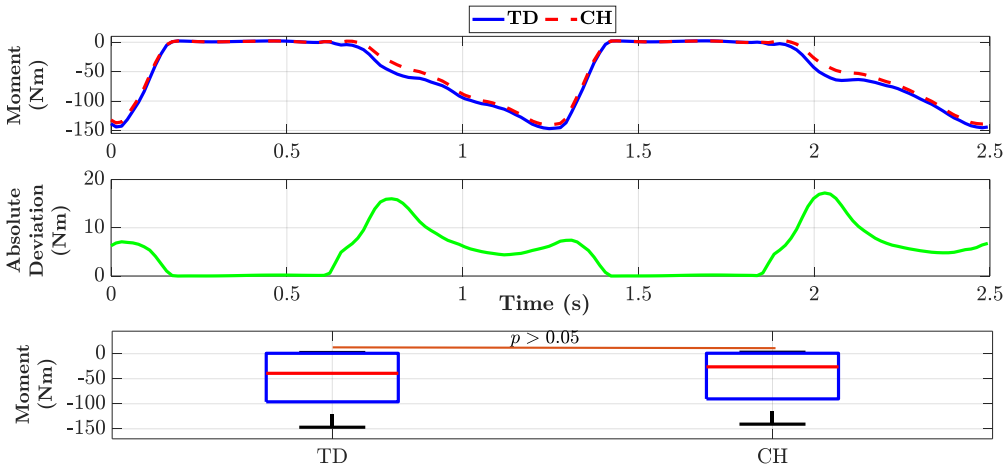

Figure 15. Comparison between TD and CH ankle moment, absolute deviation, box-plot.

3.3.6. Subtalar Moment

Figure 16 depicts the subtalar joint dynamics for both TD and CH conditions. The disparity in subtalar joint characteristics is illustrated in Figure 16, showcasing the absolute deviation between the TD and CH subtalar joint angles. The box plot analysis comparing TD and CH subtalar joint angles reveals distribution differences, as illustrated in Figure 16. In the TD subtalar joint data, the median is 10.44 Nm, with an IQR from −0.20 to 14.23 Nm, indicating a relatively moderate distribution, suggesting that the data points are somewhat spread out. The upper whisker extends to 23.63 Nm, and the lower whisker reaches −1.33 Nm, indicating some variability within the dataset. Conversely, the CH subtalar joint angles exhibit a similar distribution with a median of 10.49 Nm and an IQR from −0.20 to 15.31 Nm, suggesting that the data are spread across a similar range. The upper whisker reaches 23.86 Nm, and the lower whisker extends to −1.20 Nm, indicating slightly greater variability in the CH dataset.

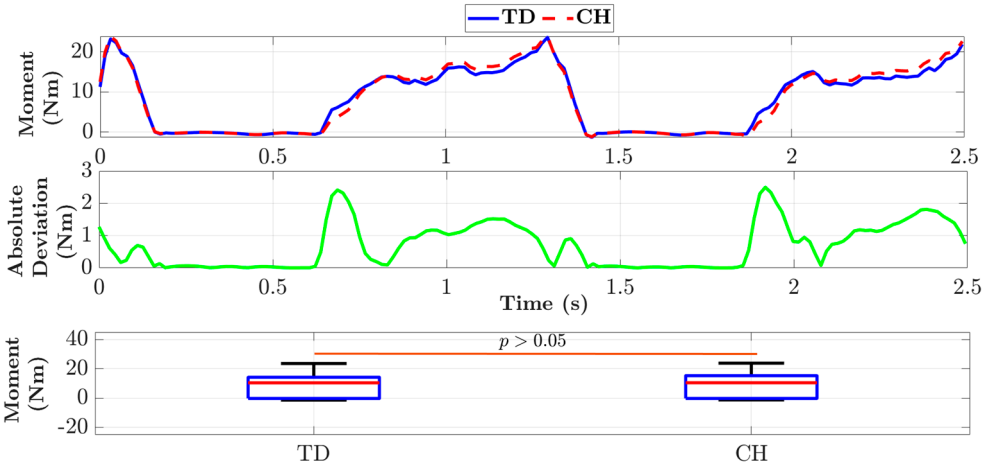

Figure 16. Comparison between TD and CH Subtalar moment, absolute deviation, and box-plot.

The *p*-values, consolidating for the above outcomes in Table 5, derived from the gait dynamics analysis provide insights into the statistical significance of differences in joint moments between typically developed (TD) individuals and contralateral hemiplegia (CH) patients. For most joint motions, including hip flexion, hip adduction, hip rotation, pelvis rotation, lumbar rotation, lumbar bending, knee flexion, ankle flexion, and subtalar flexion, $p > 0.05$ indicates no significant differences in median joint moments between the two groups. However, significant differences ($p < 0.05$) were observed in pelvis tilt and lumbar extension moments, suggesting that these motions exhibit notable biomechanical disparities between TD and CH groups. These findings emphasize the importance of focusing on pelvis and lumbar dynamics for understanding the altered mechanics in CH patients, while the lack of significant differences in other motions may indicate comparable behavior across groups for these specific joint moments.

Table 5. Statistical outcomes for TD and CH gait dynamics.

Joint and Motion	Median (TD), Nm	IQR (TD), Nm	Median (CH), Nm	IQR (CH), Nm	*p*-Value
Hip Joint					
Hip Flexion	−37.47	−44.81–12.99	−37.58	−45.82–12.14	>0.05
Hip Adduction	−9.22	−35.19–−0.48	−11.64	−36.461–1.05	>0.05
Hip Rotation	−0.99	−4.20–1.55	−0.97	−4.05–1.22	>0.05
Pelvis Bone					
Pelvis Rotation	−0.36	−6.70–5.81	−0.83	−7.48–6.20	>0.05
Pelvis Tilt	38.71	26.06–47.12	43.62	31.71–54.39	**<0.05**
Lumbar Joint					
Lumbar Extension	68.92	58.54–76.95	74.38	62.89–82.90	**<0.05**
Lumbar Rotation	0.88	−2.05–2.72	0.871	−2.29–3.07	>0.05
Lumbar Bending	5.22	−2.53–15.26	5.98	−3.30–16.89	>0.05
Knee Joint					
Knee Flexion	−6.91	−21.53–4.08	−4.07	−19.44–4.08	>0.05
Ankle Joint					
Ankle Flexion	−39.14	−96.09–0.84	−26.22	−90.24–0.95	>0.05
Subtalar Joint					
Subtalar Flexion	10.44	−0.20–14.23	10.49	−0.20–15.31	>0.05

Bold numerals in the last column represent the statistical significant conditions with significance level of 0.05.

3.4. Correlation Analysis for Joint Dynamics

The heatmaps of correlation matrices between joint dynamic parameters for TD (Figure 17a) and CH subjects (Figure 17b) reveal both similarities and differences in joint moment interactions. While some relationships remain stable, others show noticeable shifts, particularly in the coupling or decoupling of joint dynamics. The use of correlation matrices complements the boxplots and statistical analysis by offering a comprehensive view of dynamic interactions, which is crucial for understanding moment-related compensatory mechanisms in CH individuals.

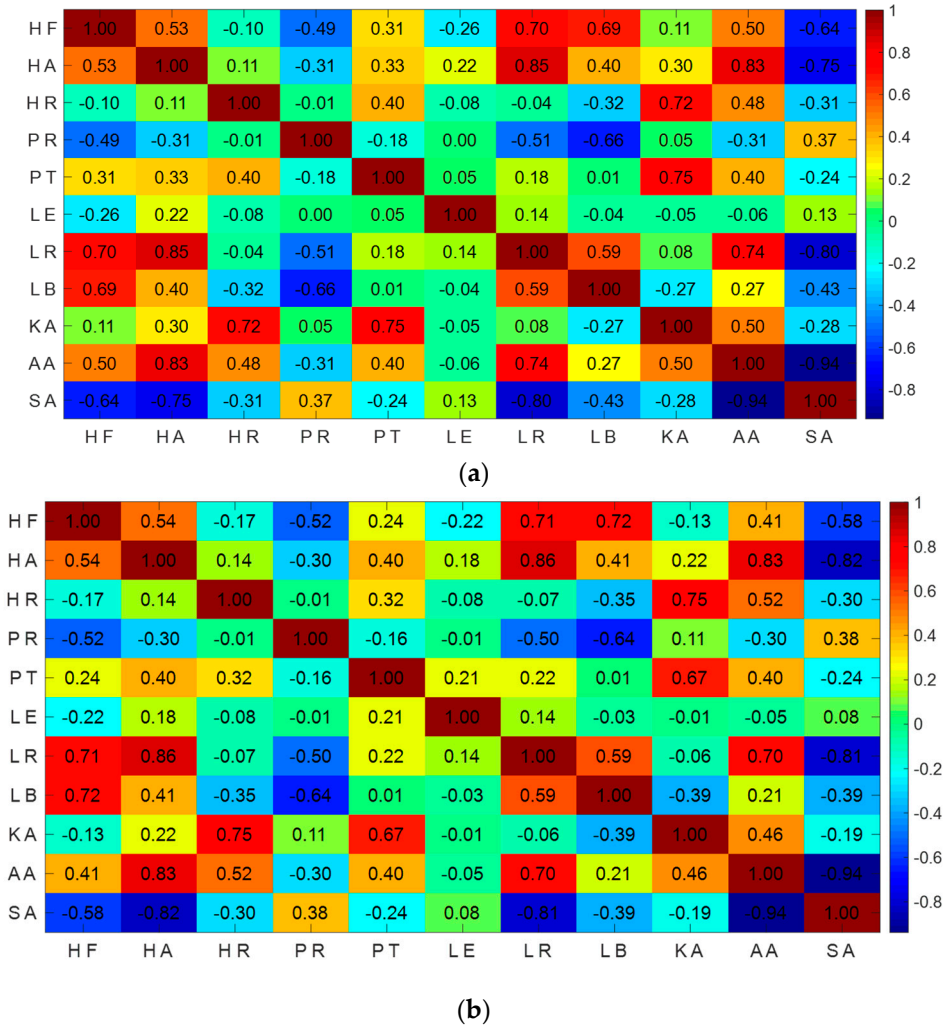

Figure 17. Correlation analysis for joint moments with (**a**) TD participants and (**b**) CH-affected subjects (− sign represents opposite phases between joints in the gait cycle).

The comparison of joint moment correlations between TD participants and CH patients reveals mostly stable interactions, with marginal differences in joint coordination patterns. For instance, the correlation between HF and HA remains consistent across both groups (0.54 in TD and 0.53 in CH), indicating preserved interaction between these joints. Similarly, the relationship between PR and LR remains stable, with correlations of −0.51 for TD participants and −0.50 for CH patients. The correlation between HF and LR also shows negligible change, shifting from 0.70 in TD to 0.71 in CH. These findings suggest that certain joint interactions, such as those involving HF, PR, and LR, are preserved regardless of health status. On the other hand, some joint correlations exhibit an increase in CH patients, indicating stronger coupling in certain movement patterns. For example, the correlation between AA and HR shows a slight increment, rising from 0.48 in TD to 0.52 in CH. Similar trends are observed in the correlations between HF and HR (−0.10 to −0.17), LB and KA (−0.27 to −0.39), HA and PT (0.33 to 0.40), and HA and SA (−0.75 to −0.82). A notable change is seen in the correlation between KA and HF, which shifts from 0.11 in TD to −0.13 in CH, reflecting altered coupling dynamics, potentially driven by compensatory strategies during movement. However, this inverse relationship suggests that these joints may operate in opposite phases during the gait cycle in CH patients, likely due to biomechanical or neuromuscular adaptations. Conversely, a few correlations show a decrease in CH patients, indicating weaker relationships in joint coordination. For example, the correlation between PT and KA reduces from 0.75 in TD to 0.67 in CH, suggesting

diminished interaction between these joints. Similarly, the correlations between SA and LB (-0.43 to -0.39), PT and HF (0.31 to 0.24), AA and HF (0.50 to 0.41), and AA and LB (0.27 to 0.21) all decrease in CH patients, pointing to weaker joint coordination and potentially altered interaction.

Overall, while certain joint interactions remain stable across TD and CH participants, others exhibit notable changes, reflecting the nuanced effects of cerebral palsy on joint coordination. Increased correlations in specific joint pairs suggest compensatory strategies to maintain functional movement, whereas decreased correlations highlight weakened relationships that may impair coordination. These shifts in joint interactions highlight how health conditions can significantly impact the biomechanical relationships between joints during motion.

4. Conclusions

This study investigated biomechanical differences in joint angles and moments between contralateral hemiplegia (CH) patients and typically developed (TD) individuals across various planes. Using OpenSim's inverse kinematics and inverse dynamics tools, lower limb joint angles and moments have been computed and compared. Statistical methods such as mean absolute deviation, box plots, *t*-tests, and correlation analysis were applied to identify significant differences. Significant differences were observed in certain joint kinematics, particularly in hip and pelvis movements. Hip flexion, pelvic tilt, lumbar extension, and ankle joint angles showed significant differences ($p < 0.05$) between TD and hemiplegic subjects, indicating altered biomechanics. In contrast, hip adduction, hip rotation, pelvis rotation, lumbar rotation, lumbar bending, knee, and subtalar joint angles and dynamics showed no significant differences ($p > 0.05$). Pelvic dynamics were mixed, with significant tilt but no notable change in rotation. The differences in joint angle correlations between TD and CH participants reveal altered motor coordination and biomechanical interactions in cerebral palsy. Stronger coupling in some joint pairs, like HR and LR, and disrupted interactions, such as PR and LR, reflect compensatory mechanisms and neuromuscular impairments in CH. While some joint interactions (moments) remain stable, others show marginal to moderate correlation shifts, highlighting the complexity of motor control in hemiplegia. These findings highlighted OpenSim's ability to identify biomechanical changes in hemiplegic patients, and are pivotal for understanding compensatory mechanisms in CH patients and provide foundational data to inform rehabilitation strategies aimed at restoring normal joint function and coordination.

This study has limitations, including the use of mean bone lengths for scaling in OpenSim models instead of subject-specific models, which may reduce the granularity of the analysis. The absence of real-time motion capture and ground reaction force data also limits the evaluation of dynamic interactions, and the relatively small, less diverse sample size may affect the generalizability of the findings. Future work should address these limitations by developing personalized musculoskeletal models to better understand joint dynamics in hemiplegic patients, particularly in the hip, pelvis, and lumbar regions. Integrating real-time motion analysis with OpenSim could enhance rehabilitation strategies, especially for pelvic tilt and lumbar extension, while expanding the study to include a larger, more diverse cohort would provide a broader understanding of hemiplegia's impact and support tailored interventions for recovery.

Author Contributions: Conceptualization, S.Y. and J.N.; methodology, J.N.; software, S.Y.; validation, S.Y., A.B. and J.N.; formal analysis, J.N., A.B. and R.M.; investigation, J.N. and R.M.; resources, J.N. and R.M.; data curation, S.Y. and J.N.; writing—original draft preparation, S.Y. and J.N.; writing—review and editing, J.N.; visualization, S.Y. and J.N.; supervision, A.B., J.N. and R.M.; project administration, A.B. and J.N. All authors have read and agreed to the published version of the manuscript.

Funding: This research received no external funding.

Institutional Review Board Statement: The study was conducted in accordance with the Declaration of Helsinki and approved by the Institutional Review Board of Indian Institute of Technology Guwahati (28 February 2020) for studies involving humans.

Informed Consent Statement: Informed consent was obtained from all subjects involved in the study.

Data Availability Statement: The original contributions presented in the study are included in the article, further inquiries can be directed to the corresponding author/s.

Acknowledgments: We thank the IIT Guwahati's physiotherapist Kandarpajyoti Das to cross validate the data obtained from the Sheosagar Paralysis and Polio Hospital in Bihar.

Conflicts of Interest: The authors declare no conflicts of interest.

References

1. Cardona, M.; Cena, C.E.G. Biomechanical analysis of the lower limb: A full-body musculoskeletal model for muscle-driven simulation. *IEEE Access* **2019**, *7*, 709–723. [CrossRef]
2. Mo, F.; Zhang, Q.; Zhang, H.; Long, J.; Wang, Y.; Chen, G.; Ye, J. A simulation-based framework with a proprioceptive musculoskeletal model for evaluating the rehabilitation exoskeleton system. *Comput. Methods Programs Biomed.* **2021**, *208*, 106270. [CrossRef] [PubMed]
3. Giarmatzis, G.; Fotiadou, S.; Giannakou, E.; Karakasis, E.; Vadikolias, K.; Aggelousis, N. Evaluating the Repeatability of Musculoskeletal Modeling Force Outcomes in Gait among Chronic Stroke Survivors: Implications for Contemporary Clinical Practice. *Biomechanics* **2024**, *4*, 333–345. [CrossRef]
4. Roelker, S.A.; Caruthers, E.J.; Baker, R.K.; Pelz, N.C.; Chaudhari, A.M.; Siston, R.A. Interpreting musculoskeletal models and dynamic simulations: Causes and effects of differences between models. *Ann. Biomed. Eng.* **2017**, *45*, 2635–2647. [CrossRef] [PubMed]
5. Kalita, B.; Narayan, J.; Dwivedy, S.K. Development of active lower limb robotic-based orthosis and exoskeleton devices: A systematic review. *Int. J. Soc. Robot.* **2021**, *13*, 775–793. [CrossRef]
6. Feigin, V.L.; Brainin, M.; Norrving, B.; Martins, S.; Sacco, R.L.; Hacke, W.; Fisher, M.; Pandian, J.; Lindsay, P. World stroke organization (wso): Global stroke fact sheet 2022. *Int. J. Stroke* **2022**, *17*, 18–29. [CrossRef]
7. North, K.; Kan, A.; De Silva, M.; Ouvrier, R. Hemiplegia due to posterior cerebral artery occlusion. *Stroke* **1993**, *24*, 1757–1760. [CrossRef] [PubMed]
8. Lazoura, O.; Papadaki, P.J.; Antoniadou, E.; Groumas, N.; Papadimitriou, A.; Thriskos, P.; Fezoulidis, I.V.; Vlychou, M. Skeletal and body composition changes in hemiplegic patients. *J. Clin. Densitom.* **2010**, *13*, 175–180. [CrossRef] [PubMed]
9. Kawakami, H.; Okuyama, O.; Liu, T. Pelvis-toe distance: 3-dimensional gait characteristics of functional limb shortening in hemiparetic stroke. *Sensors* **2021**, *21*, 5417. [CrossRef] [PubMed]
10. Riad, J.; Finnbogason, T.; Broström, E. Leg length discrepancy in spastic hemiplegic cerebral palsy: A magnetic resonance imaging study. *J. Pediatr. Orthop.* **2010**, *30*, 846–850. [CrossRef] [PubMed]
11. Gardas, S.; Shah, H. Influence of leg length discrepancy on balance and gait in post-stroke patients: A correlational study. *Bull. Fac. Phys. Ther.* **2020**, *25*, 12. [CrossRef]
12. Delp, S.L.; Anderson, F.C.; Arnold, A.S.; Loan, P.; Habib, A.; John, C.T.; Guendelman, E.; Thelen, D.G. Opensim: Open-source software to create and analyze dynamic simulations of movement. *IEEE Trans. Biomed. Eng.* **2007**, *54*, 1940–1950. [CrossRef] [PubMed]
13. Seth, A.; Hicks, J.L.; Uchida, T.K.; Habib, A.; Dembia, C.L.; Dunne, J.J.; Ong, C.F.; DeMers, M.S.; Rajagopal, A.; Millard, M.; et al. Opensim: Simulating musculoskeletal dynamics and neuromuscular control to study human and animal movement. *PLoS Comput. Biol.* **2018**, *14*, e1006223. [CrossRef] [PubMed]
14. Shachykov, A.; Frère, J.; Hénaff, P. Simulation of spinal muscle control in human gait using opensim. *IEEE Trans. Med. Robot. Bionics* **2022**, *4*, 254–265. [CrossRef]
15. Sibson, B.E.; Banks, J.J.; Yawar, A.; Yegian, A.K.; Anderson, D.E.; Lieberman, D.E. Using inertial measurement units to estimate spine joint kinematics and kinetics during walking and running. *Sci. Rep.* **2024**, *14*, 234. [CrossRef] [PubMed]
16. Sikidar, A.; Kalyanasundaram, D. An open-source opensim® anklefoot musculoskeletal model for assessment of strains and forces in dense connective tissues. *Comput. Methods Programs Biomed.* **2022**, *224*, 106994. [CrossRef] [PubMed]
17. Renganathan, G.; Barnamehei, H.; Das, S.; Kurita, Y. Effect of wearing running shoes on lower limb kinematics by using opensim simulation software. *Actuators* **2022**, *11*, 152. [CrossRef]
18. Winter, D.A. *Biomechanics and Motor Control of Human Movement*; John Wiley & Sons: Hoboken, NJ, USA, 2009.
19. Estrada-Barranco, C.; Cano-de-la-Cuerda, R.; Molina-Rueda, F. Construct validity of the Wisconsin Gait Scale in acute, subacute and chronic stroke. *Gait Posture* **2019**, *68*, 363–368. [CrossRef] [PubMed]

20. John, C.T.; Anderson, F.C.; Higginson, J.S.; Delp, S.L. Stabilisation of walking by intrinsic muscle properties revealed in a three-dimensional muscle-driven simulation. *Comput. Methods Biomech. Biomed. Eng.* **2013**, *16*, 451–462. [CrossRef]
21. Hicks, J.; Kwong, H. Getting Started with Inverse Dynamics, OpenSim Documentation. 2024. Available online: https://opensimconfluence.atlassian.net/wiki/spaces/OpenSim/pages/53090063/Getting+Started+with+Inverse+Dynamics (accessed on 6 December 2024).